PCCP

Accepted Manuscript

ROYAL SOCIETY OF CHEMISTRY

www.rsc.org/pccp

Journal Name

ARTICLE

Oxygen Vacancy as Active Site for H_2S Dissociation on Rutile TiO_2 (110) Surface: A First-principles Study

Received 00th January 20xx,
Accepted 00th January 20xx

DOI: 10.1039/x0xx00000x

www.rsc.org/

Fang Wang,[a,b] Shiqian Wei,[b] Zhi Zhang,[a] Great R. Patzke [c] and Ying Zhou[a,b*]

Abstract. Spin-polarized DFT+U computations have been performed to investigate the role of oxygen vacancy in dissociating H_2S on rutile TiO_2 (110) surface. Bridged O_{2c} atom is demonstrated to be the most energetically favorable oxygen vacancy site, which makes $V(O_{2c})$ an electron donator center and induces an isolated defect level with narrowed band gaps. H_2S molecule is adsorbed dissociatively over $V(O_{2c})$, but molecularly on the perfect surface. For H_2S dissociation, HS/H intermediate state reveals the best thermal stability on both the defected and perfect surface. Moreover, potential energy surface analysis shows that $V(O_{2c})$ reduces markedly the energy barriers for the paths along H_2S dissociation. This indicates the oxygen vacancy to be an efficient trap center for H_2S dissociation, evidenced by the significant interfacial charge transfer promoted by the vacancy. This work could provide insights into the mechanism of oxygen vacancy in facilitating the decomposition of H_2S on rutile TiO_2 (110).

1. Introduction

Hydrogen sulfide (H_2S) has long been considered as an extremely hazardous and corrosive gas which is released in large quantities generated from both nature and human factors especially in refinery of crude oil and exploitation of acid natural gas.[1-3] Industrially, Clause process has been applied to treat H_2S via $H_2S+1/2O_2 \rightarrow H_2O+S$.[4] However, this process consumes huge quantities of heat and the environmental issues associated with its by-products like SO_x are seriously concerned. Therefore, it is highly demanded to explore a green and mild strategy to eliminate H_2S. From the thermodynamic point of view, the decomposition of H_2S (39.3 kJ/mol) requires much smaller energy than that of H_2O (237.2 kJ/mol). Recently, photocatalysis technology has been proved to be a very promising way for photo-splitting H_2S via $H_2S \rightarrow H_2+S$, [5-9] which can not only reduce energy consumptions but also produce clean hydrogen energy.[10-13] However, the mechanism of H_2S adsorption and dissociation over photocatalyst surface which is the basis for H_2S-splitting has not been illuminated explicitly so far. Therefore, the related issues such as the surface reactive site, the reaction intermediates and possible reaction routes deserve in-depth investigations.

On the other hand, oxygen vacancies are the prevalent and intrinsic point defects in oxide photocatalysts[14] and play an significant role in influencing the surface charge distribution and potential energy surface of the possible channels under thermal excitation. Schaub et al.[15] demonstrated the oxygen vacancies activated the dissociation of water molecules on rutile TiO_2 (110) with strongly exothermic energy of 0.94 eV. Another very recent work reported oxygen vacancies trapped the atmospheric N_2 on the BiOBr (001) surface and facilitated the fixation of N_2 to NH_3.[16] Our previous study also revealed that oxygen vacancies in-situ formed at the polyaniline-decorated $Bi_2O_2CO_3$ (001) surface improved significantly the migration and separation of photo-induced carries.[17] Nevertheless, the role of oxygen vacancies in the interfacial interaction between H_2S and TiO_2 is barely studied.

Herein, the rutile TiO_2 (110) surface which can be obtained facilely by experiments,[18] is selected as a model material to investigate the effect of oxygen vacancies on H_2S dissociation, In addition, it also offers the opportunity to compare with the work focusing on the interaction between H_2O and rutile TiO_2 (110).[15] Huang et al.[19] reported the most possible reaction route of H_2S on the clean rutile TiO_2 (110) proceeded as $H_2S+TiO_2(110) \rightarrow S\text{-}TiO_2(110)+H_2O$. Whereas, the adsorption properties of H_2S dissociation on the defected surface have not been discussed. In this work, we investigate the electronic and energetic properties for H_2S molecular and dissociated adsorptions on the oxygen defected TiO_2 (110) as well as on the clean surface. The energy barriers for H_2S dissociation are calculated on both the defected and perfect surface. Our calculation results determine oxygen vacancy is the active surface site responsible for the dissociation of H_2S on TiO_2 (110).

2. Computational methods

[a] State Key Laboratory of Oil and Gas Reservoir Geology and Exploitation, Southwest Petroleum University, Chengdu 610500, China. E-mail: yzhou@swpu.edu.cn
[b] The Center of New Energy Materials and Technology, School of Materials Science and Engineering, Southwest Petroleum University, Chengdu 610500, China
[c] Department of Chemistry, University of Zurich, 8057 Zurich, Switzerland
† Electronic Supplementary Information (ESI) available: [Fig. S1-S6] see DOI:

First principle calculations were performed with the plane-wave pseudopotential approach implemented in the CASTEP code.[20] The electron-ion interactions were represented by the Vanderbilt Ultrasoft Pseudopotential. The cut-off energy for the plane wave basis set was 380 eV. The valence electron configurations were $3d^2 4s^2$ for Ti, $2s^2 2p^4$ for O, $3s^2 3p^4$ for S, and $1s^1$ for H, respectively. A Hubbard-like correction, was introduced to the localized density approximation LDA/CA-PZ,[21, 22] usually called LDA+U,[23] and was used to describe the exchange correlation effects and electron-electron interactions, due to the underestimation of coulomb repulsion for the d or f orbitals of transition metals in the density functional theory (DFT). Ortmann–Bechstedt–Schmidt dispersion corrected method[24] was applied to describe properly the van der Waals interactions in the system. Extensive tests for the appropriate U parameter were carried out to get a band gap close to bulk rutile TiO_2 (3.05 eV),[25] which was found to be 9.0 eV for Ti 3d as supplemented in Fig. S1 for brevity. The same U value was also used for LDA calculations of graphene/Anatse TiO_2 (001) system.[26] Monkhorst-Pack *k*-points 3×3×5 in the Brillouin-zone were used for the bulk TiO_2. The geometry optimization stopped until the residual force was below 0.01 eV/ Å for all relaxed atoms. The predicted crystal constants were $a=b=4.55$ Å and $c=2.92$ Å, which reproduced well with the experimental data.[27] A stoichiometric (2×1) slab with four atomic layers was built to interact with H_2S, as was used in the previous theoretical work.[19] Two bottom layers were fixed at the bulk position. 2×2×1 *k*-points were used for surface optimizations. A vacuum space of 15 Å was set to separate the interaction between the periodic images. Spin polarization and dipole correction were applied for all calculations.

As displayed in Fig. 1, three kinds of oxygen atoms on the surface lead to various oxygen vacancy sites. The formation energy of oxygen vacancy (E_f) was calculated as follows:

$$E_f = E_{surf}(TiO_{2-x}) - [E_{surf}(TiO_2) - 1/2E(O_2)] \quad (1)$$

where $E_{surf}(TiO_{2-x})$, $E_{surf}(TiO_2)$ and $E(O_2)$ were total energies for the oxygen defected surface, the pure surface and the chemical potential of O_2, respectively. The more positive E_f is, the more difficult to form oxygen vacancy.

The atomic and fragmental difference charge density (Δρ) were calculated by Eq 2 and 3, respectively.

$$\Delta\rho = \rho(slab) - [\rho(Ti) + \rho(O)] \quad (2)$$

$$\Delta\rho = \rho(adsorbate+slab) - [\rho(slab) + \rho(adsorbate)] \quad (3)$$

where ρ(slab), ρ(Ti) and ρ(O) were the charge densities of the slab, Ti and O atoms, respectively. ρ(adsorbate+slab), ρ(slab) and ρ(adsorbate) were the charge densities of the adsorbed system, slab and adsorbate, respectively.

The surface energy (E_{surf}) for the perfect surface was calculated as follows:

$$E_{surf} = [E_{surf}(TiO_2) - nE_{bulk}(TiO_2)]/2S \quad (4)$$

where $E_{surf}(TiO_2)$, $E_{bulk}(TiO_2)$, N, and S were the total energies for the perfect surface and TiO_2 bulk, the number of TiO_2 bulk in the perfect surface and the surface area of supercell, respectively.

H_2S isolated molecule was optimized in a vacuum box of 10Å×10Å×10Å. The predicted bond length and bond angel were 1.35 Å and 91.34°, respectively, which agreed well with the parameters reported in the previous work.[28] The adsorption behaviors were investigated by the interfacial interactions of H_2S and its fragments HS/S and S/H/H with surface respectively. The adsorption energy (E_{ads}) was calculated using the equation:

$$E_{ads} = E(adsorbate+slab) - [E(slab) + E(adsorbate)] \quad (2)$$

Transition states (TS) were located by using the complete LST/QST method.[29] Firstly, the linear synchronous transit (LST) maximization was performed, followed by an energy minimization in directions conjugated to the reaction pathway. Secondly, the TS approximation obtained in that way was used to perform quadratic synchronous transit (QST) maximization. Then, another conjugated gradient minimization was performed. The cycle was repeated until a stationary point was located. The energy barrier is defined as the energy difference between the transition state and reactants.

In the preliminary calculations, the energy convergence of the clean slab with respect to the supercell size was computed and was supplemented in Fig. S2. The variation trend of surface energies and H_2S adsorption energies were almost in a straight line with the increasing (2×1), (2×2) and (2×3) perfect supercells, ca. 0.13 eV/Å^2 and 1.71 eV, respectively. This suggested the (2×1) slab was sufficient to provide a good representation of the surface properties and was used in the study. Additionally, H_2S adsorption energies for (2×1) perfect slab became slightly negative and differed by less than 0.1 eV with U value ranging from 7, 8, 9, 10, 11 to 12 eV. Moreover, energy profiles of H_2S dissociation on the perfect slab were similar using different U values (Fig. S3), indicating the selected U of 9 eV was appropriate to provide reliable energies. Based on the selected slab and U value, we further tested the feasibility of the LDA method compared to the generalized gradient approximation GGA/PW91[30] functional including the dispersion correction[24] (Fig. S4). The energy profiles of H_2S dissociation shifted positively for GGA method relative to LDA results, and the energy barriers were close and varied by less than 0.1 eV. Therefore, the dispersion corrected LDA method can get reliable results and was applied in the calculations.

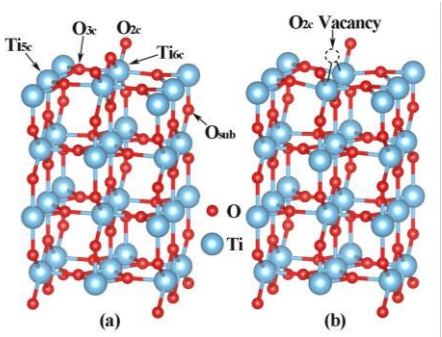

Fig. 1 Optimized geometries of the perfect surface (a) and (b) the defective surface.

3. Results and Discussion

3.1 Structural Relaxation and Electronic Structure of Rutile TiO_2 (110) surface

The TiO_2 (110) surface is terminated by bridging oxygen atoms (O_{2c}) arranging along the [001] direction as illustrated in Fig. 1. The atomic displacements after relaxation for the perfect surface as well as the measured values are summarized in Table 1. A positive value indicates the upward atomic movement along the *z*-axis, and the negative value means the downward movement. The atomic relaxations of all atoms accord well with surface X-ray diffraction (SXRD) observations,[31] indicating our calculation model is reliable. As can be found in Table 1, the formation energies of possible oxygen vacancies obey the order: $E_f(O_{2c}) < E_f(O_{3c}) < E_f(O_{sub})$, which is consistent with the calculated result of Matsunaga et al.[32] Thus, the O_{2c} vacancy $V(O_{2c})$ is selected as the optimal surface point defect to explore the influence on the physiochemical properties of rutile TiO_2 (110).

Table 1 The predicted atom relaxation of perfect TiO_2 (110) surface along the *z*-axis together with experimental data[a] and the calculated oxygen vacancy formation energies.

Atom	SXRD[31]	This Work	
	Perfect Surface(Å)	Perfect Surface(Å)	Oxygen vacancy Formation (eV)
O_{2c}	-0.27±0.08	-0.007	4.15
O_{3c}	0.05±0.05	0.152	4.53
O_{sub}	0.05±0.08	-0.002	5.05
Ti_{5c}	-0.16±0.05	-0.158	
Ti_{6c}	0.12±0.05	0.193	

[a] Experimental data taken from Ref. 31.

Upon the introduction of $V(O_{2c})$, we note obvious structural changes and most of the surface atoms move downward. This indicates the surface shrinks to reduce the surface free energy. A striking point is that Ti_{6c} atom has a displacement of 0.127 Å along the [100] direction, resulting in the Ti_{6c}-Ti_{6c} distance stretching from 2.92 Å to 3.18 Å (Fig. 2). To understand the reason for the atomic movements, Mulliken population analysis was performed to examine the surface charge redistribution. It is found that the net charges of atoms near $V(O_{2c})$ become more negative compared to the perfect surface. The localization of the excess charge on Ti_{6c} atoms may apart the two Ti_{6c} atoms, as proposed by Morgan et. al.[33] The electron density variation can be observed intuitively from the charge density difference maps displayed in Fig. 2. The introduction of $V(O_{2c})$ results in an evident electron accumulation around the two Ti_{6c} atoms, indicating the unpaired electrons left by the loss of O_{2c} transfers to the neighboring Ti_{6c} atoms. This makes the $V(O_{2c})$ site an electron donator center to be an active surface site, which plays an important role in the physiochemical properties of TiO_2 surfaces.[34]

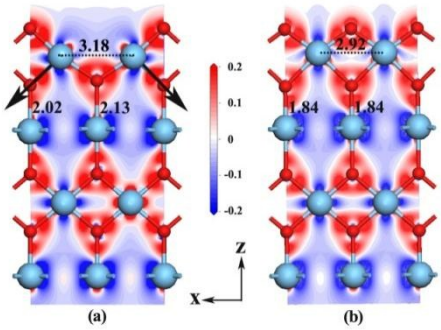

Fig. 2. The difference charge densities of the defected surface (a) and the perfect surface (b). The bond length and charge density are in Å and electrons/Å^3 respectively.

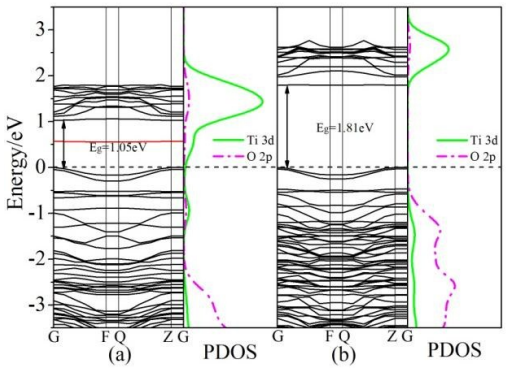

Fig. 3 The band structures and PDOS of the defected surface (a) and the perfect surface (b), respectively.

Fig. 3 shows the band structures of defected rutile TiO_2 (110) as well as the perfect surface. According to the partial density of states (PDOS), the defected surface has the same band contribution with the perfect surface, i.e., the valence bands are mainly contributed from O 2p states and the conduction bands are primarily constructed by Ti 3d states. But it exhibits a narrowed band gap with the conduction bands shifting to the low energy regions. One remarkable point is the appearance of an isolated defect energy level, mainly composed of Ti 3d across the band gap, which is in accord with the experimental observations.[35] The defect level could promote the photo-induced electron-hole separation.[36, 37]

3.2 H_2S Dissociation on Rutile TiO_2 (110)

To study H_2S dissociation reactions ($H_2S \rightarrow HS\cdot + H\cdot$, $HS\cdot \rightarrow S + H\cdot$) on rutile TiO_2 (110), adsorption energies of H_2S and its dissociated products for the first and second steps, namely HS/H and S/H/H on the defected surface as well as the perfect surface are investigated and displayed in Fig. 4. It is noted that an equivalent perfect surface containing a Ti_{5c} atom at the surface center is considered as the energetically favorable adsorbed surface, evidenced by the previous theoretical study[19] and scanning tunneling microscope imaging.[15] Interestingly, once H_2S is adsorbed over $V(O_{2c})$, it spontaneously dissociates into HS/H on the surface. This means the H_2S molecule is adsorbed dissociatively over the defected surface without energy barrier required. In contrast, H_2S adsorbs molecularly on the perfect surface with the adsorption energy of -1.71 eV. Namely, $V(O_{2c})$ favors H_2S

dissociation on the surface. The adsorption energies of HS/H and S/H/H over V(O_{2c}) are -2.48 and -2.16 eV respectively, which are more negative than that of over the Ti_{5c} site on the perfect surface. In addition, HS/H intermediate has the relative lower adsorption energies for both the defected and perfect surfaces, which is consistent with the study on H_2S dissociation on metal surfaces.[28] However, it is different from H_2O dissociation on perfect rutile TiO_2 (110), which shows the molecular adsorption is more energetically favorable relative to the dissociated states.[15] This proves H_2S dissociates facilely on the rutile TiO_2 (110) compared to H_2O in accord with the thermodynamic theory.

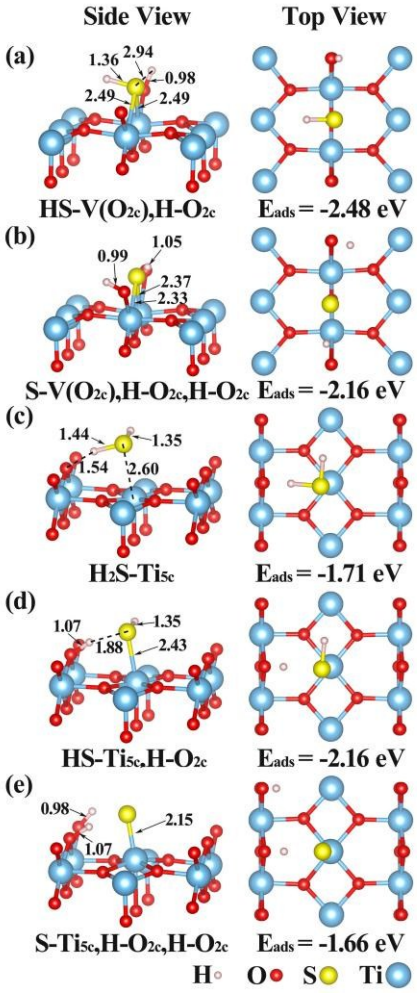

Fig. 4 Molecular and dissociated adsorption configurations. HS/H (a) and S/H/H (b) on the defected surface, H_2S (c), HS/H (d) and S/H/H (e) on the perfect surface respectively. The bond length is in Å.

To confirm V(O_{2c}) to be an active site for H_2S dissociation, the potential energy surface for the path along dissociation is calculated and plotted in Fig. 5. The TS configurations are supplemented in Fig. S5. H_2S spontaneously dissociates into HS/H over V(O_{2c}), and requires an energy barrier of 1.4 eV to decompose into S/H/H. Whereas much higher energy barriers are needed for H_2S dissociation on the perfect surface, 0.61 and 3.19 eV for the first and second step respectively. Therefore, V(O_{2c}) may act as the efficient trap for H_2S dissociation. The smaller energy barriers also provides theoretical evidence for much easier dissociation of H_2S than that of H_2O over V(O_{2c}) on rutile TiO_2 (110),[15] which is in agreement with the experimental results.[13]

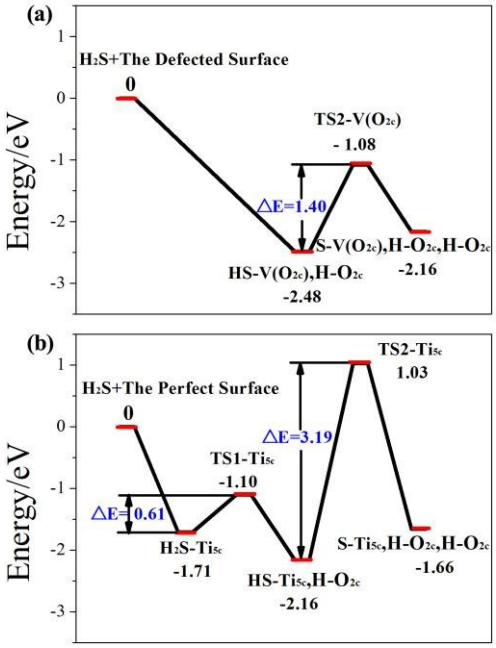

Fig. 5 Energy profiles for H_2S dissociation on the defected surface (a) and the perfect surface (b) respectively.

To gain insights into the adsorption configurations and the interfacial integrations, we investigated the adsorption properties in detail. It is seen from Fig. 4a for the dissociated state HS/H, one proton of H_2S transfers to the nearby oxygen atom and forms one O-H bond of 0.98 Å. Upon on the second-dissociation step (Fig. 4b), the S atom is firmly absorbed at the V(O_{2c}) site, forming two Ti-S bonds reducing from 2.49 to ca. 2.35 Å. This means a more covalent bond character. While the bond length of Ti-S bond is slightly longer than that of Ti-O bond due to the larger atomic radius of S atom. The formation of OH groups result in significant elongation of Ti-O bond, suggesting the Ti-O bonds are activated and favor the removing of OH groups from the surface. For H_2S molecular adsorption on the perfect surface (Fig. 4c), the S atom is attracted by the Ti_{5c}, and a SH···OTi hydrogen bond has formed by 1.54 Å. During the dissociation process, the OH groups and Ti-S bond are formed as well as the defected surface (Figs. 4d and 4e).

The interfacial bonding interactions were further investigated by PDOS as shown in Fig. 6. For HS/H adsorption on the defected surface, Fig. 6a illustrates that the peaks of S 2p and Ti 3d orbits locate at the same energy level at the top of valence bands, indicating the covalent feature of Ti-S bond. Meanwhile, H 1s and O 2p hybrid at ca. -6.7, -7.6 and -7.8 eV respectively, which suggests the formation of H-O hydrogen bond and renders the HS/H intermediate energetically favorable due to the stabilization of hydrogen bonding effect.

This is also evidenced by its largest adsorption energy magnitude. After the dissociation of HS, the distinct peaks composed of O 2p and H 1s at the deep valence region become more evident as shown in Fig. 6b. This demonstrates the formation of hydroxyl groups on the surface. Besides, S 2p state splits into two characteristic peaks and overlaps with Ti 3d at the top of valence band. However, O 2p state shifts significantly to the deep valence region. This indicates the electron transition route has been changed after H_2S dissociation on the defected surface, i.e., electron transfers from S 2p to Ti 3d compared to O 2p to Ti 3d for the defected surface, which promotes significantly the interfacial charge transfer. Similar state hybridizations between S and Ti, H and O can also be found in the PDOS of H_2S dissociation on the perfect surface.

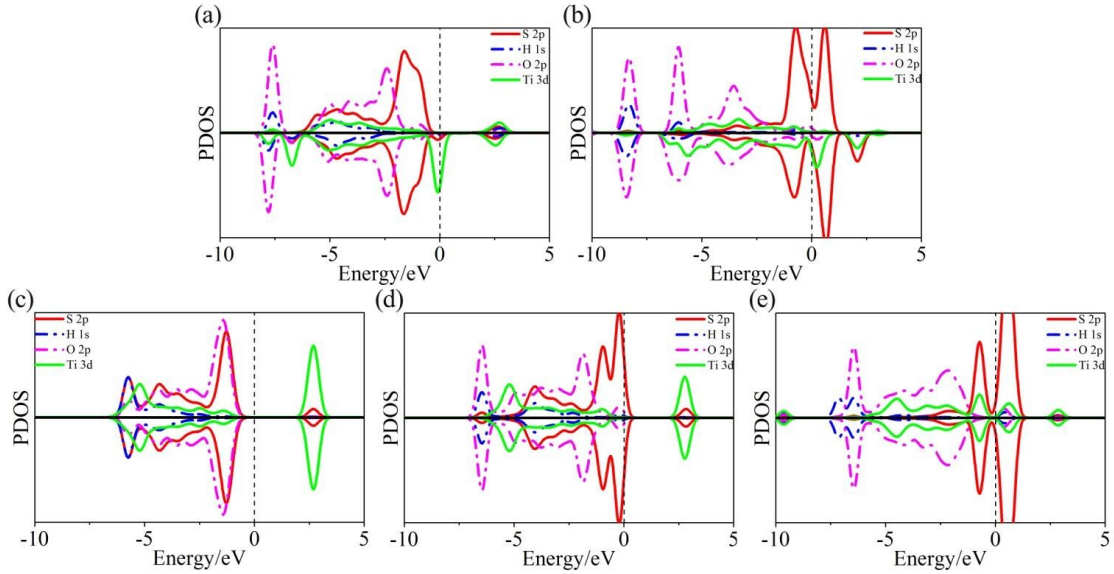

Fig. 6 The PDOS of HS/H (a) and S/H/H (b) on the defected surface, and H_2S (c), HS/H (d) and S/H/H (e) on the perfect surface, respectively.

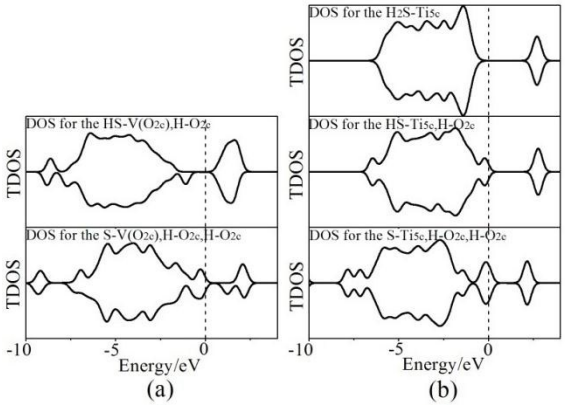

Fig. 7 TDOS maps for HS/H and S/H/H adsorbed defected surface (a), and H_2S, HS/H and S/H/H adsorbed on the perfect surface (b), respectively.

In view of TDOS (total density of states) maps in Fig. 7a, it is interesting to note that a spin-down peak shows up across the Fermi level for HS/H adsorbed over $V(O_{2c})$. Whereas after HS dissociation, a spin-up peak appears at the same energy level and results in an almost symmetrical state which is composed by Ti 3d and S 2p, suggesting the defect energy level induced by $V(O_{2c})$ has disappeared. This is due to the formation of the covalent Ti-S bond which shares the unpaired electron left by the removal oxygen atom. While for the H_2S dissociation on the perfect surface, a symmetrical state also occurs at the Fermi level (Fig. 7b). All in all, upon H_2S dissociation, an symmetrical gap state forms across the Fermi level due to the state hybridization of S 2p and Ti 3d, which could promote the charge transfer and enhance the interfacial interactions.[38]

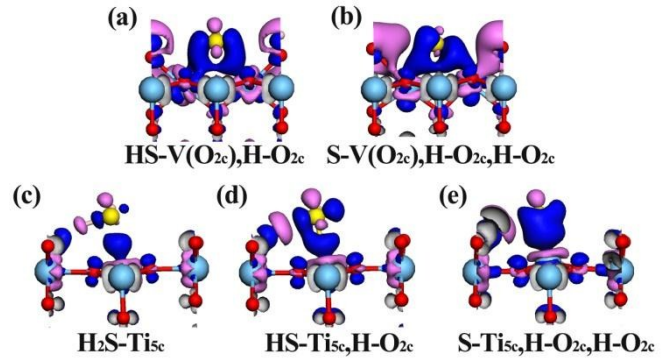

Fig. 8 The difference charge densities of HS/H (a) and S/H/H (b) on the defected surface, and H_2S (c), HS/H (d) and S/H/H (e) on the perfect surface, respectively. Pink areas represent electron depletion and blue areas means electron accumulation with an isosurface value of 0.05 electrons/Å^3.

The interfacial charge transfer is investigated by the difference charge density in Fig. 8. For HS/H dissociation over $V(O_{2C})$ (Fig. 8a), electrons accumulate mainly between S and the adjacent two Ti atoms, and minorly between H and O atoms, indicating electrons transfer from Ti to S and H to O at the interface. With the dissociation of HS, more electrons have assembled between S and Ti atoms as shown in Fig. 8b,

indicating stronger covalent Ti-S bond. While for H_2S dissociation on the perfect surface, we note fewer electrons gather between Ti and S at the surface. Additionally, total electron density maps supplemented in Fig. S6 illustrates a larger cloud area of electron density at the interface for H_2S dissociation over $V(O_{2c})$, which proves stronger interfacial interactions between the sulfur adsorbates and surface. Therefore, $V(O_{2c})$ indeed significantly promotes the interfacial charge transfer as was found by previous work[16, 17] and facilitates the breakdown of H_2S on the surface.

4. Conclusions

In this work, we have performed dispersion corrected spin-polarized DFT+U calculations to investigate the role of oxygen vacancy in H_2S dissociation on the rutile TiO_2 (110) surface. The optimal oxygen vacancy site $V(O_{2c})$ is at the bridged O_{2c} atom and induces an isolated defect level within the band gap. Adsorption analysis shows that HS/H state has the best thermal stability for both the defected and perfect surfaces. Upon H_2S adsorption over $V(O_{2c})$, it dissociates directly into HS/H, and a small energy barrier of 1.4 eV is required for further decomposition into S/H/H. But for H_2S dissociation on the perfect surface, it has to overcome much higher energy barriers along each channel. Moreover, larger areas of electron accumulation locates over $V(O_{2c})$ at the interface. Based on the calculation results, we determine $V(O_{2c})$ to be an active site in facilitating H_2S dissociation on the surface.

Acknowledgements

We gratefully acknowledge financial support from Open Fund of State Key Laboratory of Oil and Gas Reservoir Geology and Exploitation (PLN1522), the Sino Swiss Science and Technology Cooperation (SSSTC, EG08-032015), Scientific Research Starting Project of SWPU (2014QHZ020, 2014PYZ012), the Innovative Research Team of Sichuan Province and SWPU (2016TD0011, 2012XJZT002), and College Students' Extracurricular Open Experiment Project of SWPU (KSZ15101).

Notes and references

1 A. Davoodi, M. Babaiee and M. Pakshir, *Met. Mater. Int.*, 2013, **19**, 731-740.
2 M. A. Migahed, A. M. Al-Sabagh, E. G. Zaki, H. A. Mostafa and A. S. Fouda, *Int. J. Electrochem. Sc.*, 2014, **9**, 7693-7711.
3 A. Alonso-Tellez, D. Robert, N. Keller and V. Keller, *Appl. Catal. B-Environ.*, 2012, **115**, 209-218.
4 A. Vrachnos, G. Kontogeorgis and E. Voutsas, *Ind. Eng. Chem. Res.*, 2006, **45**, 5148-5154.
5 J. S. Lee, *Cataly. Surv. Asia*, 2006, **9**, 217-227.
6 K. Maeda and K. Domen, *J. Phys. Chem. C*, 2007, **111**, 7851-7861.
7 F. E. Osterloh, *Chem. Mater.*, 2008, **20**, 35-54.
8 J. Ran, J. Zhang, J. Yu, M. Jaroniec and S. Z. Qiao, *Chem. Soc. Rev.*, 2014, **43**, 7787-7812.
9 S. Bashir, A. K. Wahab and H. Idriss, *Catal. Today*, 2015, **240**, 242-247.
10 J. S. Jang, H. G. Kim, P. H. Borse and J. S. Lee, *Int. J. Hydrogen Energ.*, 2007, **32**, 4786-4791.
11 N. S. Chaudhari, S. S. Warule, S. A. Dhanmane, M. V. Kulkarni, M. Valant and B. B. Kale, *Nanoscale*, 2013, **5**, 9383-9390.
12 N. S. Chaudhari, A. P. Bhirud, R. S. Sonawane, L. K. Nikam, S. S. Warule, V. H. Rane and B. B. Kale, *Green Chem.*, 2011, **13**, 2500-2506.
13 U. V. Kawade, R. P. Panmand, Y. A. Sethi, M. V. Kulkarni, S. K. Apte, S. D. Naik and B. B. Kale, *RSC Adv.*, 2014, **4**, 49295-49302.
14 G. U. Von Oertzen and A. R. Gerson, *Int. J. Quantum Chem.*, 2006, **106**, 2054-2064.
15 R. Schaub, P. Thostrup, N. Lopez, E. Lægsgaard, I. Stensgaard, J. K. Nørskov and F. Besenbacher, *Phys. Rev. Lett.*, 2001, **87**, 266140.
16 H. Li, J. Shang, Z. Ai and L. Zhang, *J. Am. Chem. Soc.*, 2015, **137**, 6393-6399.
17 Z. Zhao, Y. Zhou, F. Wang, K. Zhang, S. Yu and K. Cao, *ACS Appl. Mater. Inter.*, 2015, **7**, 730-737.
18 M. H. M. Ahmed, F. P. Lydiatt, D. Chekulaev, P. L. Wincott, D. J. Vaughan, J. H. Jang, S. Baldelli, A. G. Thomas, W. S. Walters and R. Lindsay, *Surf. Sci.*, 2014, **630**, 41-45.
19 W. F. Huang, H. T. Chen and M. C. Lin, *J. Phys. Chem. C*, 2009, **113**, 20411-20420.
20 M. D. Segall, P. J. D. Lindan, M. J. Probert, C. J. Pickard, P. J. Hasnip, S. J. Clark and M. C. Payne, *J. Phys.- Condens. Mat.*, 2002, **14**, 2717-2744.
21 D. M. Ceperley and B. J. Alder, *Phys. Rev. Lett.*, 1980, **45**, 566-569.
22 J. P. Perdew and A. Zunger, *Phys. Rev. B*, 1981, **23**, 5048.
23 A. I. Liechtenstein, V. I. Anisimov and J. Zaanen, *Phys. Rev. B*, 1995, **52**, R5467.
24 F. Ortmann, F. Bechstedt and W. G. Schmidt, *Phys. Rev. B*, 2006, **73**, 205101.
25 J. Pascual, J. Camassel and H. Mathieu, *Phys. Rev. B*, 1978, **18**, 5606-5614.
26 H. Gao, X. Li, J. Lv and G. Liu, *J. Phys. Chem. C*, 2013, **117**, 16022-16027.
27 X. Bokhimi, A. Morales and F. Pedraza, *J. Solid State Chem.*, 2002, **169**, 176-181.
28 S. Chen, S. Sun, B. Lian, Y. Ma, Y. Yan and S. Hu, *Surf. Sci.*, 2014, **620**, 51-58.
29 T. A. Halgren and W. N. Lipscomb, *Chem. Phys. Lett.*, 1977, **49**, 225-232.
30 J. P. Perdew, J. A. Chevary, S. H. Vosko, K. A. Jackson, M. R. Pederson, D. J. Singh and C. Fiolhais, *Phys. Rev. B*, 1992, **46**, 6671-6687.
31 G. Charlton, P. B. Howes, C. L. Nicklin, P. Steadman, J. S. G. Taylor, C. A. Muryn, S. P. Harte, J. Mercer, R. McGrath and D. Norman, *Phys. Rev. Lett.*, 1997, **78**, 495.
32 K. Matsunaga, Y. Tanaka, K. Toyoura, A. Nakamura, Y. Ikuhara and N. Shibata, *Phys. Rev. B*, 2014, **90**, 195303.
33 B. J. Morgan and G. W. Watson, *Surf. Sci.*, 2007, **601**, 5034-5041.
34 P. Krüger, S. Bourgeois, B. Domenichini, H. Magnan, D. Chandesris, P. Le Fevre, A. M. Flank, J. Jupille, L. Floreano and A. Cossaro, *Phys. Rev. lett.*, 2008, **100**, 055501.
35 V. Henrich, G. Dresselhaus and H. Zeiger, *Phys. Rev. Lett.*, 1976, **36**, 1335-1339.
36 H. Zhang, L. Liu and Z. Zhou, *RSC Adv.*, 2012, **2**, 9224-9229.
37 D. Li, H. Haneda, N. K. Labhsetwar, S. Hishita and N. Ohashi, *Chem. Phys. Lett.*, 2005, **401**, 579-584.
38 J. A. Rodriguez, J. Hrbek, Z. Chang, J. Dvorak, T. Jirsak and A. Maiti, *Phys. Rev. B*, 2002, **65**, 235414.